Chiral 2π exchange at fourth order and peripheral NN scattering

D. R. Entem* and R. Machleidt†
Department of Physics, University of Idaho, Moscow, Idaho 83844
(Received 14 February 2002; published 17 July 2002)

We calculate the impact of the complete set of two-pion exchange contributions at chiral fourth order (also known as next-to-next-to-next-to-leading order) on peripheral partial waves of nucleon-nucleon scattering. Our calculations are based upon the analytical studies by Kaiser. It turns out that the contribution of fourth order is substantially smaller than the one of third order, indicating convergence of the chiral expansion. We compare the prediction from chiral pion exchange with the corresponding one from conventional meson theory as represented by the Bonn full model and find, in general, good agreement. Our calculations provide a sound basis for investigating the issue whether the low-energy constants determined from πN lead to reasonable predictions for NN.

DOI: 10.1103/PhysRevC.66.014002 PACS number(s): 13.75.Cs, 21.30.Cb, 12.38.Bx

I. INTRODUCTION

One of the most fundamental problems of nuclear physics is a proper derivation of the force between two nucleons. A great obstacle for the solution of this problem has been the fact that the fundamental theory of strong interaction, QCD, is nonperturbative in the low-energy regime characteristic for nuclear physics. The way out of this dilemma is paved by the effective field theory concept which recognizes different energy scales in nature. Below the chiral symmetry breaking scale, $\Lambda_\chi \approx 1$ GeV, the appropriate degrees of freedom are pions and nucleons interacting via a force that is governed by the symmetries of QCD, particularly (broken) chiral symmetry.

The derivation of the nuclear force from chiral effective field theory was initiated by Weinberg [1] and pioneered by Ordóñez, Ray, and van Kolck [2–4]. Subsequently, many researchers became interested in the field [5–20]. As a result, efficient methods for deriving the nuclear force from chiral Lagrangians emerged [7–12] and the quantitative nature of the chiral nucleon-nucleon (NN) potential improved [13,14].

Current NN potentials [13,14] and phase shift analyses [21] include 2π-exchange contributions up to third order in small momenta [next-to-next-to-leading order (NNLO)]. However, the contribution at third order is very large, several times the one at second order (NLO). This fact raises serious questions concerning the convergence of the chiral expansion for the two-nucleon problem. Moreover, it was shown in Ref. [14] that a *quantitative* chiral NN potential requires contact terms of fourth order. Consistency then implies that also 2π (and 3π) contributions are to be included up to fourth order.

For the reasons discussed, it is a timely project to investigate the chiral 2π-exchange contribution to the NN interaction at fourth order. Recently, Kaiser [11,12] has derived the analytic expressions at this order using covariant perturbation theory and dimensional regularization. It is the chief purpose of this paper to apply these contributions in peripheral NN scattering and compare the predictions to empirical phase shifts as well as to the results from conventional meson theory. Furthermore, we will investigate the above-mentioned convergence issue. Our calculations provide a sound basis to discuss the question whether the low-energy constants (LECs) determined from πN lead to reasonable predictions in NN.

In Sec. II, we summarize the Lagrangians involved in the evaluation of the 2π-exchange contributions presented in Sec. III. In Sec. IV, we explain how we calculate the phase shifts for peripheral partial waves and present results. Section V concludes the paper.

II. EFFECTIVE CHIRAL LAGRANGIANS

The effective chiral Lagrangian relevant to our problem can be written as [22,23]

$$\mathcal{L}_{\rm eff} = \mathcal{L}^{(2)}_{\pi\pi} + \mathcal{L}^{(1)}_{\pi N} + \mathcal{L}^{(2)}_{\pi N} + \mathcal{L}^{(3)}_{\pi N} + \cdots, \tag{1}$$

where the superscript refers to the number of derivatives or pion mass insertions (chiral dimension) and the ellipsis stands for terms of chiral fourth order or higher.

At lowest and leading order, the $\pi\pi$ Lagrangian is given by

$$\mathcal{L}^{(2)}_{\pi\pi} = \frac{f_\pi^2}{4}{\rm tr}[\partial^\mu U \partial_\mu U^\dagger + m_\pi^2 (U + U^\dagger)] \tag{2}$$

and the relativistic πN Lagrangian reads

$$\mathcal{L}^{(1)}_{\pi N} = \bar{\Psi}\left(i\gamma^\mu D_\mu - M_N + \frac{g_A}{2}\gamma^\mu \gamma_5 u_\mu \right)\Psi, \tag{3}$$

with

$$D_\mu = \partial_\mu + \Gamma_\mu, \tag{4}$$

$$\Gamma_\mu = \frac{1}{2}(\xi^\dagger \partial_\mu \xi + \xi \partial_\mu \xi^\dagger) = \frac{i}{4f_\pi^2}\boldsymbol{\tau}\cdot(\boldsymbol{\pi}\times\partial_\mu\boldsymbol{\pi}) + \cdots, \tag{5}$$

*On leave from University of Salamanca, Spain. Electronic address: dentem@uidaho.edu
†Electronic address: machleid@uidaho.edu

$$u_\mu = i(\xi^\dagger \partial_\mu \xi - \xi \partial_\mu \xi^\dagger) = -\frac{1}{f_\pi}\boldsymbol{\tau}\cdot\partial_\mu\boldsymbol{\pi} + \cdots, \tag{6}$$

$$U = \xi^2 = 1 + \frac{i}{f_\pi}\boldsymbol{\tau}\cdot\boldsymbol{\pi} - \frac{1}{2f_\pi^2}\boldsymbol{\pi}^2 - \frac{i\alpha}{f_\pi^3}(\boldsymbol{\tau}\cdot\boldsymbol{\pi})^3 + \frac{8\alpha-1}{8f_\pi^4}\boldsymbol{\pi}^4 + \cdots. \tag{7}$$

The coefficient α that appears in the last equation is arbitrary. Therefore, diagrams with chiral vertices that involve three or four pions must always be grouped together such that the α dependence drops out (cf. Fig. 3, below).

In the above equations, M_N denotes the nucleon mass, g_A the axial-vector coupling constant, and f_π the pion decay constant. Numerical values are given in Table I.

We apply the heavy baryon (HB) formulation of chiral perturbation theory [28] in which the relativistic πN Lagrangian is subjected to an expansion in terms of powers of $1/M_N$ (kind of a nonrelativistic expansion), the lowest order of which is

$$\hat{\mathcal{L}}^{(1)}_{\pi N} = \overline{N}\left(iD_0 - \frac{g_A}{2}\vec{\sigma}\cdot\vec{u}\right)N$$
$$= \overline{N}\left[i\partial_0 - \frac{1}{4f_\pi^2}\boldsymbol{\tau}\cdot(\boldsymbol{\pi}\times\partial_0\boldsymbol{\pi}) - \frac{g_A}{2f_\pi}\boldsymbol{\tau}\cdot(\vec{\sigma}\cdot\vec{\nabla})\boldsymbol{\pi}\right]N + \cdots. \tag{8}$$

In the relativistic formulation, the field operators representing nucleons, Ψ, contain four-component Dirac spinors, while in the HB version, the field operators N contain Pauli spinors; in addition, all nucleon field operators contain Pauli spinors describing the isospin of the nucleon.

At dimension 2, the relativistic πN Lagrangian reads

$$\mathcal{L}^{(2)}_{\pi N} = \sum_{i=1}^{4} c_i \overline{\Psi} O_i^{(2)} \Psi. \tag{9}$$

The various operators $O_i^{(2)}$ are given in Ref. [23]. The fundamental rule by which this Lagrangian—as well as all the other ones—is assembled is that it must contain *all* terms consistent with chiral symmetry and Lorentz invariance (apart from the other trivial symmetries) at a given chiral dimension (here, order 2). The parameters c_i are known as LECs and are determined empirically from fits to πN data (Table I).

The HB projected πN Lagrangian at second order is most conveniently broken up into two pieces,

$$\hat{\mathcal{L}}^{(2)}_{\pi N} = \hat{\mathcal{L}}^{(2)}_{\pi N,\mathrm{fix}} + \hat{\mathcal{L}}^{(2)}_{\pi N,\mathrm{ct}}, \tag{10}$$

with

$$\hat{\mathcal{L}}^{(2)}_{\pi N,\mathrm{fix}} = \overline{N}\left[\frac{1}{2M_N}\vec{D}\cdot\vec{D} + i\frac{g_A}{4M_N}\{\vec{\sigma}\cdot\vec{D}, u_0\}\right]N \tag{11}$$

and

TABLE I. Parameters used in our calculations. The LECs c_i and $\overline{d_i}$ are in units of GeV^{-1} and GeV^{-2}, respectively.

	Our choice	Empirical
M_N	938.9182 MeV	
m_π	138.039 MeV	
g_A	1.29	1.29 ± 0.01[a]
f_π	92.4 MeV	92.4 ± 0.3 MeV[b]
c_1	−0.81	-0.81 ± 0.15[c]
c_2	3.28	3.28 ± 0.23[d]
c_3	−3.40	-4.69 ± 1.34[c]
c_4	3.40	3.40 ± 0.04[c]
$\overline{d_1}+\overline{d_2}$	3.06	3.06 ± 0.21[d]
$\overline{d_3}$	−3.27	-3.27 ± 0.73[d]
$\overline{d_5}$	0.45	0.45 ± 0.42[d]
$\overline{d_{14}}-\overline{d_{15}}$	−5.65	-5.65 ± 0.41[d]

[a]Using $g^2_{\pi NN}/4\pi = 13.63\pm0.20$ [24,25] and applying the Goldberger-Treiman relation, $g_A = g_{\pi NN} f_\pi / M_N$.
[b]Reference [26].
[c]Table 1, fit 1 of Ref. [27].
[d]Table 2, fit 1 of Ref. [22].

$$\hat{\mathcal{L}}^{(2)}_{\pi N,\mathrm{ct}} = \overline{N}\left[2c_1 m_\pi^2 (U+U^\dagger) + \left(c_2 - \frac{g_A^2}{8M_N}\right)u_0^2 + c_3 u_\mu u^\mu + \frac{i}{2}\left(c_4 + \frac{1}{4M_N}\right)\vec{\sigma}\cdot(\vec{u}\times\vec{u})\right]N. \tag{12}$$

Note that $\hat{\mathcal{L}}^{(2)}_{\pi N,\mathrm{fix}}$ is created entirely from the HB expansion of the relativistic $\mathcal{L}^{(1)}_{\pi N}$ and thus has no free parameters ("fixed"), while $\hat{\mathcal{L}}^{(2)}_{\pi N,\mathrm{ct}}$ is dominated by the new πN contact terms proportional to the c_i parameters, besides some small $1/M_N$ corrections.

At dimension 3, the relativistic πN Lagrangian can be formally written as

$$\mathcal{L}^{(3)}_{\pi N} = \sum_{i=1}^{23} d_i \overline{\Psi} O_i^{(3)} \Psi, \tag{13}$$

with the operators, $O_i^{(3)}$, listed in Refs. [22,23]; not all 23 terms are of interest here. The new LECs that occur at this order are the d_i. Similar to the second-order case, the HB projected Lagrangian at third order can be broken into two pieces,

$$\hat{\mathcal{L}}^{(3)}_{\pi N} = \hat{\mathcal{L}}^{(3)}_{\pi N,\mathrm{fix}} + \hat{\mathcal{L}}^{(3)}_{\pi N,\mathrm{ct}}, \tag{14}$$

with $\hat{\mathcal{L}}^{(3)}_{\pi N,\mathrm{fix}}$ and $\hat{\mathcal{L}}^{(3)}_{\pi N,\mathrm{ct}}$ given in Refs. [22,23].

III. NONITERATIVE 2π-EXCHANGE CONTRIBUTIONS TO THE *NN* INTERACTION

The effective Lagrangian presented in the previous section is the crucial ingredient for the evaluation of the pion-exchange contributions to the nucleon-nucleon (NN) interaction. Since we are dealing here with a low-energy effective

theory, it is appropriate to analyze the diagrams in terms of powers of small momenta: $(Q/\Lambda_\chi)^\nu$, where Q stands for a momentum (nucleon three-momentum or pion four-momentum) or a pion mass and $\Lambda_\chi \approx 1$ GeV is the chiral symmetry breaking scale. This procedure has become known as power counting. For noniterative contributions to the NN interaction (i.e., irreducible graphs with four external nucleon legs), the power ν of a diagram is given by

$$\nu = 2l + \sum_j \left(d_j + \frac{n_j}{2} - 2 \right), \tag{15}$$

where l denotes the number of loops in the diagram, d_j the number of derivatives or pion-mass insertions and n_i the number of nucleon fields involved in vertex j; the sum runs over all vertices j contained in the diagram under consideration.

At zeroth order [$\nu=0$, lowest order, leading order (LO)], we have only the static one-pion-exchange (OPE) and, at first order, there are no pion-exchange contributions. Higher-order graphs are shown in Figs. 1–3. Analytic results for these graphs were derived by Kaiser and co-workers [7,11,12] using covariant perturbation; i.e., they start out with the relativistic versions of the πN Lagrangians (see previous section). Relativistic vertices and nucleon propagators are then expanded in powers of $1/M_N$. The divergences that occur in conjunction with the four-dimensional loop integrals are treated by means of dimensional regularization, a prescription which is consistent with chiral symmetry and power counting. The results derived in this way are the same obtained when starting right away with the HB versions of the πN Lagrangians. However, as it turns out, the method used by the Munich group is more efficient in dealing with the rather tedious calculations.

We will state the analytical results in terms of contributions to the on-shell momentum-space NN amplitude which has the general form

$$\begin{aligned} V(\vec{p}\,',\vec{p}) = \frac{1}{(2\pi)^3}\{ & V_C + \boldsymbol{\tau}_1\cdot\boldsymbol{\tau}_2 W_C + [V_S + \boldsymbol{\tau}_1\cdot\boldsymbol{\tau}_2 W_S]\vec{\sigma}_1\cdot\vec{\sigma}_2 \\ & + [V_T + \boldsymbol{\tau}_1\cdot\boldsymbol{\tau}_2 W_T]\vec{\sigma}_1\cdot\vec{q}\,\vec{\sigma}_2\cdot\vec{q} \\ & + [V_{LS} + \boldsymbol{\tau}_1\cdot\boldsymbol{\tau}_2 W_{LS}](-i\vec{S}\cdot(\vec{q}\times\vec{k})) \\ & + [V_{\sigma L} + \boldsymbol{\tau}_1\cdot\boldsymbol{\tau}_2 W_{\sigma L}]\vec{\sigma}_1\cdot(\vec{q}\times\vec{k})\vec{\sigma}_2\cdot(\vec{q}\times\vec{k})\}, \end{aligned} \tag{16}$$

where $\vec{p}\,'$ and $\vec{p}$ denote the final and initial nucleon momenta in the center-of-mass (c.m.) frame, respectively,

$$\vec{q} \equiv \vec{p}\,' - \vec{p} \quad \text{is the momentum transfer,}$$

$$\vec{k} \equiv \frac{1}{2}(\vec{p}\,' + \vec{p}) \quad \text{the average momentum,}$$

$$\vec{S} \equiv \frac{1}{2}(\vec{\sigma}_1 + \vec{\sigma}_2) \quad \text{the total spin,}$$

and $\vec{\sigma}_{1,2}$ and $\boldsymbol{\tau}_{1,2}$ are the spin and isospin operators, respectively, of nucleons 1 and 2. For on-energy-shell scattering, V_α and W_α ($\alpha = C,S,T,LS,\sigma L$) can be expressed as functions of q and k (with $q \equiv |\vec{q}|$ and $k \equiv |\vec{k}|$), only.

Our formalism is similar to the one used in Refs. [7–12], except for two differences: all our momentum-space amplitudes differ by an overall factor of (-1) and our spin-orbit amplitudes V_{LS} and W_{LS} differ by an additional factor of (-2) from the conventions used by Kaiser *et al.* [7–12]. We have chosen our conventions such that they are closely in tune with what is commonly used in nuclear physics.

We stress that, throughout this paper, we consider *on-shell* NN amplitudes; i.e., we always assume $|\vec{p}\,'| = |\vec{p}| \equiv p$. Note also that we will state only the *nonpolynomial* part of the amplitudes. Polynomial terms can be absorbed into contact interactions that are not the subject of this study. Moreover, in Sec. IV, below, we will show results for NN scattering in F and higher partial waves (orbital angular momentum $L \geqslant 3$) where polynomials of order Q^ν with $\nu \leqslant 4$ do not contribute.

A. Second order

Two-pion exchange occurs first at second order ($\nu=2$, NLO), also know as leading-order 2π exchange. The graphs are shown in the first row of Fig. 1. Since a loop creates already $\nu=2$, the vertices involved at this order can only be from the leading and lowest-order Lagrangian $\hat{\mathcal{L}}^{(1)}_{\pi N}$, Eq. (8); i.e., they carry only one derivative. These vertices are denoted by small dots in Fig. 1. Note that, here, we include only the noniterative part of the box diagram which is obtained by subtracting the iterated OPE contribution [Eq. (64), below, but using $M_N^2/E_p \approx M_N$] from the full box diagram at second order. To make this paper self-contained and to uniquely define the contributions for which we will show results in Sec. IV, below, we summarize here the explicit mathematical expressions derived in Ref. [7]:

$$W_C = -\frac{L(q)}{384\pi^2 f_\pi^4}\left[4m_\pi^2(5g_A^4 - 4g_A^2 - 1) + q^2(23g_A^4 - 10g_A^2 - 1) + \frac{48 g_A^4 m_\pi^4}{w^2} \right], \tag{17}$$

$$V_T = -\frac{1}{q^2} V_S = -\frac{3g_A^4 L(q)}{64\pi^2 f_\pi^4}, \tag{18}$$

where

$$L(q) \equiv \frac{w}{q} \ln \frac{w+q}{2m_\pi} \tag{19}$$

and

$$w \equiv \sqrt{4m_\pi^2 + q^2}. \tag{20}$$

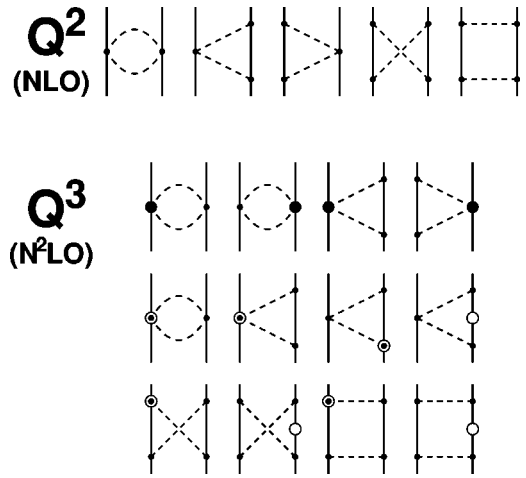

FIG. 1. Two-pion exchange contributions to the *NN* interaction at second and third order in small momenta. Solid lines represent nucleons and dashed lines pions. Small dots denote vertices from the leading order πN Lagrangian $\hat{\mathcal{L}}^{(1)}_{\pi N}$, Eq. (8). Large solid dots are vertices proportional to the LECs c_i from the second-order Lagrangian $\hat{\mathcal{L}}^{(2)}_{\pi N,\mathrm{ct}}$, Eq. (12). Symbols with open circles are relativistic $1/M_N$ corrections contained in the second-order Lagrangian $\hat{\mathcal{L}}^{(2)}_{\pi N}$, Eqs. (10). Only a few representative examples of $1/M_N$ corrections are shown and not all.

B. Third order

The two-pion-exchange diagrams of third order ($\nu=3$, NNLO) are very similar to the ones of second order, except that they contain one insertion from $\hat{\mathcal{L}}^{(2)}_{\pi N}$, Eq. (10). The resulting contributions are typically either proportional to one of the low-energy constants c_i or they contain a factor $1/M_N$. Notice that relativistic $1/M_N$ corrections can occur for vertices and nucleon propagators. In Fig. 1, we show in row 2 the diagrams with vertices proportional to c_i (large solid dot), Eq. (12), and in rows 3 and 4 a few representative graphs with a $1/M_N$ correction (symbols with an open circle). The number of $1/M_N$ correction graphs is large and not all are shown in the figure. Again, the box diagram is corrected for a contribution from the iterated OPE: in Eq. (64), below, the expansion of the factor $M_N^2/E_p = M_N - p^2/M_N + \cdots$ is applied; the term proportional to $(-p^2/M_N)$ is subtracted from the third-order box diagram contribution. For completeness, we recall here the mathematical expressions derived in Ref. [7]:

$$V_C = \frac{3g_A^2}{16\pi f_\pi^4}\left\{\frac{g_A^2 m_\pi^5}{16M_N w^2} - \left[2m_\pi^2(2c_1-c_3) - q^2\left(c_3+\frac{3g_A^2}{16M_N}\right)\right]\tilde{w}^2 A(q)\right\}, \tag{21}$$

$$W_C = \frac{g_A^2}{128\pi M_N f_\pi^4}\{3g_A^2 m_\pi^5 w^{-2} - [4m_\pi^2 + 2q^2 - g_A^2(4m_\pi^2+3q^2)]\tilde{w}^2 A(q)\}, \tag{22}$$

$$V_T = -\frac{1}{q^2}V_S = \frac{9g_A^4\tilde{w}^2 A(q)}{512\pi M_N f_\pi^4}, \tag{23}$$

$$W_T = -\frac{1}{q^2}W_S = -\frac{g_A^2 A(q)}{32\pi f_\pi^4}\left[\left(c_4+\frac{1}{4M_N}\right)w^2 - \frac{g_A^2}{8M_N}(10m_\pi^2+3q^2)\right], \tag{24}$$

$$V_{LS} = \frac{3g_A^4\tilde{w}^2 A(q)}{32\pi M_N f_\pi^4}, \tag{25}$$

$$W_{LS} = \frac{g_A^2(1-g_A^2)}{32\pi M_N f_\pi^4}w^2 A(q), \tag{26}$$

with

$$A(q) \equiv \frac{1}{2q}\arctan\frac{q}{2m_\pi} \tag{27}$$

and

$$\tilde{w} \equiv \sqrt{2m_\pi^2+q^2}. \tag{28}$$

C. Fourth order

This order, which may also be denoted by next-to-next-to-next-to-leading order ($\mathrm{N^3LO}$), is the main focus of this paper. There are one-loop graphs (Fig. 2) and two-loop contributions (Fig. 3).

1. One-loop diagrams

(*a*) c_i^2 *contributions*. The only contribution of this kind comes from the football diagram with both vertices proportional to c_i (first row of Fig. 2). One obtains [11]

$$V_C = \frac{3L(q)}{16\pi^2 f_\pi^4}\left[\left(\frac{c_2}{6}w^2 + c_3\tilde{w}^2 - 4c_1 m_\pi^2\right)^2 + \frac{c_2^2}{45}w^4\right], \tag{29}$$

$$W_T = -\frac{1}{q^2}W_S = \frac{c_4^2 w^2 L(q)}{96\pi^2 f_\pi^4}. \tag{30}$$

(*b*) c_i/M_N *contributions*. This class consists of diagrams with one vertex proportional to c_i and one $1/M_N$ correction. A few graphs that are representative for this class are shown in the second row of Fig. 2. Symbols with a large solid dot and an open circle denote $1/M_N$ corrections of vertices proportional to c_i. They are part of $\hat{\mathcal{L}}^{(3)}_{\pi N}$, Eq. (14). The result for this group of diagrams is [11]

$$V_C = -\frac{g_A^2 L(q)}{32\pi^2 M_N f_\pi^4}[(c_2-6c_3)q^4 + 4(6c_1+c_2-3c_3)q^2 m_\pi^2 + 6(c_2-2c_3)m_\pi^4 + 24(2c_1+c_3)m_\pi^6 w^{-2}], \tag{31}$$

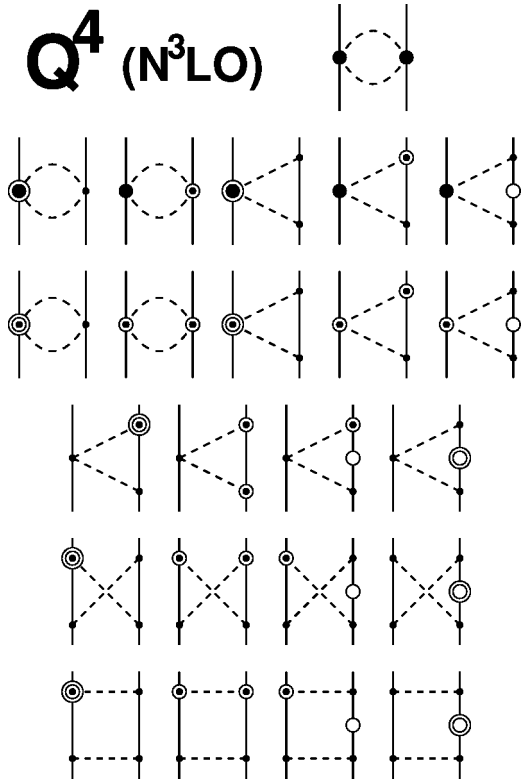

FIG. 2. One-loop 2π-exchange contributions to the NN interaction at fourth order. Basic notation as in Fig. 1. Symbols with a large solid dot and an open circle denote $1/M_N$ corrections of vertices proportional to c_i. Symbols with two open circles mark relativistic $1/M_N^2$ corrections. Both corrections are part of the third-order Lagrangian $\hat{\mathcal{L}}_{\pi N}^{(3)}$, Eq. (14). Representative examples for all types of one-loop graphs that occur at this order are shown.

$$W_C = -\frac{c_4 q^2 L(q)}{192\pi^2 M_N f_\pi^4}[g_A^2(8m_\pi^2+5q^2)+w^2], \tag{32}$$

$$W_T = -\frac{1}{q^2}W_S = -\frac{c_4 L(q)}{192\pi^2 M_N f_\pi^4}[g_A^2(16m_\pi^2+7q^2)-w^2], \tag{33}$$

$$V_{LS} = \frac{c_2 g_A^2}{8\pi^2 M_N f_\pi^4} w^2 L(q), \tag{34}$$

$$W_{LS} = -\frac{c_4 L(q)}{48\pi^2 M_N f_\pi^4}[g_A^2(8m_\pi^2+5q^2)+w^2]. \tag{35}$$

(c) $1/M_N^2$ *corrections*. These are relativistic $1/M_N^2$ corrections of the leading-order 2π-exchange diagrams. Typical examples for this large class are shown in rows 3–6 of Fig. 2. This time, there is no correction from the iterated OPE, Eq. (64), since the expansion of the factor M_N^2/E_p does not create a term proportional to $1/M_N^2$. The total result for this class is [12]

$$V_C = -\frac{g_A^4}{32\pi^2 M_N^2 f_\pi^4}\Bigg[L(q)(2m_\pi^8 w^{-4} + 8m_\pi^6 w^{-2} - q^4 - 2m_\pi^4) + \frac{m_\pi^6}{2w^2}\Bigg], \tag{36}$$

$$W_C = -\frac{1}{768\pi^2 M_N^2 f_\pi^4}\Bigg\{L(q)\Bigg[8g_A^2\Bigg(\frac{3}{2}q^4+3m_\pi^2 q^2+3m_\pi^4 - 6m_\pi^6 w^{-2} - k^2(8m_\pi^2+5q^2)\Bigg) + 4g_A^4[k^2(20m_\pi^2+7q^2 - 16m_\pi^4 w^{-2}) + 16m_\pi^8 w^{-4} + 12m_\pi^6 w^{-2} - 4m_\pi^4 q^2 w^{-2} - 5q^4 - 6m_\pi^2 q^2 - 6m_\pi^4] - 4k^2 w^2\Bigg] + \frac{16 g_A^4 m_\pi^6}{w^2}\Bigg\}, \tag{37}$$

$$V_T = -\frac{1}{q^2}V_S = \frac{g_A^4 L(q)}{32\pi^2 M_N^2 f_\pi^4}\Bigg(k^2+\frac{5}{8}q^2+m_\pi^4 w^{-2}\Bigg), \tag{38}$$

$$W_T = -\frac{1}{q^2}W_S = \frac{L(q)}{1536\pi^2 M_N^2 f_\pi^4}\Bigg[4g_A^4\Bigg(7m_\pi^2+\frac{17}{4}q^2 + 4m_\pi^4 w^{-2}\Bigg) - 32g_A^2\Bigg(m_\pi^2+\frac{7}{16}q^2\Bigg)+w^2\Bigg], \tag{39}$$

$$V_{LS} = \frac{g_A^4 L(q)}{4\pi^2 M_N^2 f_\pi^4}\Bigg(\frac{11}{32}q^2+m_\pi^4 w^{-2}\Bigg), \tag{40}$$

$$W_{LS} = \frac{L(q)}{256\pi^2 M_N^2 f_\pi^4}\Bigg[16g_A^2\Bigg(m_\pi^2+\frac{3}{8}q^2\Bigg) + \frac{4}{3}g_A^4\Bigg(4m_\pi^4 w^{-2} - \frac{11}{4}q^2 - 9m_\pi^2\Bigg) - w^2\Bigg], \tag{41}$$

$$V_{\sigma L} = \frac{g_A^4 L(q)}{32\pi^2 M_N^2 f_\pi^4}. \tag{42}$$

In the above expressions, we have replaced the p^2 dependence used in Ref. [12] by a k^2 dependence applying the (on-shell) identity

$$p^2 = \frac{1}{4}q^2 + k^2. \tag{43}$$

2. Two-loop contributions

The two-loop contributions are quite involved. In Fig. 3, we attempt a graphical representation of this class. The gray disk stands for all one-loop πN graphs which are shown in some detail in the lower part of the figure. Not all of the numerous graphs are displayed. Some of the missing ones are obtained by permutation of the vertices along the nucleon line, others by inverting initial and final states. Vertices denoted by a small dot are from the leading-order πN Lagrang-

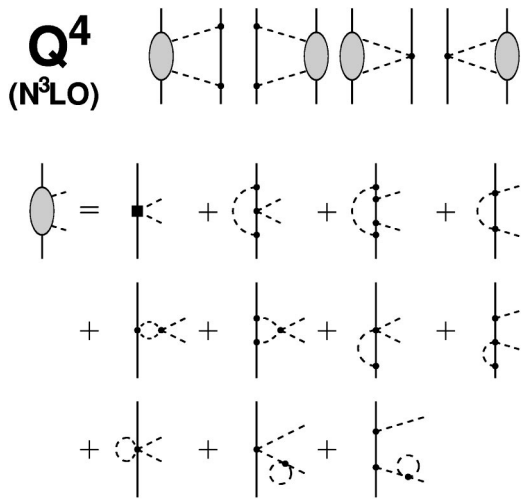

FIG. 3. Two-loop 2π-exchange contributions at fourth order. Basic notation as in Fig. 1. The oval stands for all one-loop πN graphs some of which are shown in the lower part of the figure. The solid square represents vertices proportional to the LECs d_i which are introduced by the third-order Lagrangian $\mathcal{L}^{(3)}_{\pi N}$, Eq. (13). More explanations are given in the text.

ian $\hat{\mathcal{L}}^{(1)}_{\pi N}$, Eq. (8), except for the 4π vertices which are from $\mathcal{L}^{(2)}_{\pi\pi}$, Eq. (2). The solid square represents vertices proportional to the LECs d_i which are introduced by the third-order Lagrangian $\mathcal{L}^{(3)}_{\pi N}$, Eq. (13). The d_i vertices occur actually in one-loop NN diagrams, but we list them among the two-loop NN contributions because they are needed to absorb divergences generated by one-loop πN graphs. Using techniques from dispersion theory, Kaiser [11] calculated the imaginary parts of the NN amplitudes, $\mathrm{Im}\,V_\alpha(i\mu)$ and $\mathrm{Im}\,W_\alpha(i\mu)$, which result from analytic continuation to timelike momentum transfer $q=i\mu-0^+$ with $\mu\geqslant 2m_\pi$. We will first state these expressions and, then, further elaborate on them:

$$\mathrm{Im}\,V_C(i\mu)=-\frac{3g_A^4(\mu^2-2m_\pi^2)}{\pi\mu(4f_\pi)^6}\Bigg[(m_\pi^2-2\mu^2)\times\left(2m_\pi+\frac{2m_\pi^2-\mu^2}{2\mu}\ln\frac{\mu+2m_\pi}{\mu-2m_\pi}\right)+4g_A^2m_\pi(2m_\pi^2-\mu^2)\Bigg], \tag{44}$$

$$\mathrm{Im}\,W_C(i\mu)=\mathrm{Im}\,W_C^{(a)}(i\mu)+\mathrm{Im}W_C^{(b)}(i\mu), \tag{45}$$

with

$$\mathrm{Im}\,W_C^{(a)}(i\mu)=-\frac{2\kappa}{3\mu(8\pi f_\pi^2)^3}\int_0^1 dx\Big[g_A^2(2m_\pi^2-\mu^2)+2(g_A^2-1)\kappa^2x^2\Big]\Big\{96\pi^2f_\pi^2\Big[(2m_\pi^2-\mu^2)\times(\overline{d}_1+\overline{d}_2)-2\kappa^2x^2\overline{d}_3+4m_\pi^2\overline{d}_5\Big]+\Big[4m_\pi^2(1+2g_A^2)-\mu^2(1+5g_A^2)\Big]\frac{\kappa}{\mu}\times\ln\frac{\mu+2\kappa}{2m_\pi}+\frac{\mu^2}{12}(5+13g_A^2)-2m_\pi^2(1+2g_A^2)\Big\} \tag{46}$$

and

$$\mathrm{Im}\,W_C^{(b)}(i\mu)=-\frac{2\kappa}{3\mu(8\pi f_\pi^2)^3}\int_0^1 dx\Big[g_A^2(2m_\pi^2-\mu^2)+2(g_A^2-1)\kappa^2x^2\Big]\Big\{-3\kappa^2x^2+6\kappa x\sqrt{m_\pi^2+\kappa^2x^2}\ln\frac{\kappa x+\sqrt{m_\pi^2+\kappa^2x^2}}{m_\pi}+g_A^4(\mu^2-2\kappa^2x^2-2m_\pi^2)\left[\frac{5}{6}+\frac{m_\pi^2}{\kappa^2x^2}-\left(1+\frac{m_\pi^2}{\kappa^2x^2}\right)^{3/2}\ln\frac{\kappa x+\sqrt{m_\pi^2+\kappa^2x^2}}{m_\pi}\right]\Big\}, \tag{47}$$

$$\mathrm{Im}\,V_S(i\mu)=\mathrm{Im}\,V_S^{(a)}(i\mu)+\mathrm{Im}\,V_S^{(b)}(i\mu)=\mu^2\mathrm{Im}\,V_T(i\mu)=\mu^2\mathrm{Im}\,V_T^{(a)}(i\mu)+\mu^2\mathrm{Im}\,V_T^{(b)}(i\mu) \tag{48}$$

with

$$\mathrm{Im}\,V_S^{(a)}(i\mu)=\mu^2\mathrm{Im}\,V_T^{(a)}(i\mu)=-\frac{3g_A^2\mu\kappa^3}{16\pi f_\pi^4}\int_0^1 dx(1-x^2)(\overline{d}_{14}-\overline{d}_{15}) \tag{49}$$

and

$$\mathrm{Im}\,V_S^{(b)}(i\mu)=\mu^2\mathrm{Im}\,V_T^{(b)}(i\mu)=-\frac{2g_A^6\mu\kappa^3}{(8\pi f_\pi^2)^3}\int_0^1 dx(1-x^2)\left[-\frac{1}{6}+\frac{m_\pi^2}{\kappa^2x^2}-\left(1+\frac{m_\pi^2}{\kappa^2x^2}\right)^{3/2}\ln\frac{\kappa x+\sqrt{m_\pi^2+\kappa^2x^2}}{m_\pi}\right], \tag{50}$$

$$\mathrm{Im}\, W_S(i\mu) = \mu^2 \mathrm{Im} W_T(i\mu) = -\frac{g_A^4(\mu^2-4m_\pi^2)}{\pi(4f_\pi)^6}\left[\left(m_\pi^2-\frac{\mu^2}{4}\right)\times \ln\frac{\mu+2m_\pi}{\mu-2m_\pi}+(1+2g_A^2)\mu m_\pi\right], \quad (51)$$

where $\kappa \equiv \sqrt{\mu^2/4-m_\pi^2}$.

We need the momentum-space amplitudes $V_\alpha(q)$ and $W_\alpha(q)$ which can be obtained from the above expressions by means of the dispersion integrals:

$$V_{C,S}(q) = -\frac{2q^6}{\pi}\int_{2m_\pi}^{\infty} d\mu \frac{\mathrm{Im}\ V_{C,S}(i\mu)}{\mu^5(\mu^2+q^2)}, \quad (52)$$

$$V_T(q) = \frac{2q^4}{\pi}\int_{2m_\pi}^{\infty} d\mu \frac{\mathrm{Im}\ V_T(i\mu)}{\mu^3(\mu^2+q^2)}, \quad (53)$$

and similarly for $W_{C,S,T}$.

We have evaluated these dispersion integrals and obtain

$$V_C(q) = \frac{3g_A^4\tilde{w}^2A(q)}{1024\pi^2 f_\pi^6}\{(m_\pi^2+2q^2)[2m_\pi+\tilde{w}^2A(q)] + 4g_A^2 m_\pi \tilde{w}^2\}, \quad (54)$$

$$W_C(q) = W_C^{(a)}(q) + W_C^{(b)}(q) \quad (55)$$

with

$$W_C^{(a)}(q) = \frac{L(q)}{18432\pi^4 f_\pi^6}\left\{192\pi^2 f_\pi^2 w^2 \overline{d}_3\left[2g_A^2\tilde{w}^2 - \frac{3}{5}(g_A^2-1)w^2\right] + [6g_A^2\tilde{w}^2-(g_A^2-1)w^2] \times\left[384\pi^2 f_\pi^2[\tilde{w}^2(\overline{d}_1+\overline{d}_2)+4m_\pi^2\overline{d}_5] + L(q)[4m_\pi^2(1+2g_A^2)+q^2(1+5g_A^2)] - \left(\frac{q^2}{3}(5+13g_A^2)+8m_\pi^2(1+2g_A^2)\right)\right]\right\} \quad (56)$$

and

$$W_C^{(b)}(q) = -\frac{2q^6}{\pi}\int_{2m_\pi}^{\infty} d\mu \frac{\mathrm{Im}\ W_C^{(b)}(i\mu)}{\mu^5(\mu^2+q^2)}, \quad (57)$$

$$V_T(q) = V_T^{(a)}(q) + V_T^{(b)}(q) = -\frac{1}{q^2}V_S(q) = -\frac{1}{q^2}[V_S^{(a)}(q)+V_S^{(b)}(q)], \quad (58)$$

with

$$V_T^{(a)}(q) = -\frac{1}{q^2}V_S^{(a)}(q) = -\frac{g_A^2 w^2 L(q)}{32\pi^2 f_\pi^4}(\overline{d}_{14}-\overline{d}_{15}) \quad (59)$$

and

$$V_T^{(b)}(q) = -\frac{1}{q^2}V_S^{(b)}(q) = \frac{2q^4}{\pi}\int_{2m_\pi}^{\infty} d\mu \frac{\mathrm{Im}\ V_T^{(b)}(i\mu)}{\mu^3(\mu^2+q^2)}, \quad (60)$$

$$W_T(q) = -\frac{1}{q^2}W_S(q) = \frac{g_A^4 w^2 A(q)}{2048\pi^2 f_\pi^6}[w^2A(q)+2m_\pi(1+2g_A^2)]. \quad (61)$$

We were able to find analytic solutions for all dispersion integrals except $W_C^{(b)}$ and $V_T^{(b)}$ (and $V_S^{(b)}$). The analytic solutions hold modulo polynomials. We have checked the importance of those contributions where the integrations have to be performed numerically. It turns out that the combined effect on NN phase shifts from $W_C^{(b)}$, $V_T^{(b)}$, and $V_S^{(b)}$ is smaller than 0.1° in F and G waves and smaller than 0.01° in H waves, at $T_{\mathrm{lab}}=300$ MeV (and less at lower energies). This renders these contributions negligible, a fact that may be of interest in future chiral NN potential developments where computing time could be an issue. We stress, however, that in all phase shift calculations of this paper (presented in Sec. IV, below) the contributions from $W_C^{(b)}$, $V_T^{(b)}$, and $V_S^{(b)}$ are always included in all fourth-order results.

In Eqs. (56) and (59), we use the scale-independent LECs, $\overline{d}_i$, which are obtained by combining the scale-dependent ones $d_i^r(\lambda)$ with the chiral logarithmus $\ln(m_\pi/\lambda)$ or, equivalently, $\overline{d}_i = d_i^r(m_\pi)$. The scale-dependent LECs $d_i^r(\lambda)$ are a consequence of renormalization. For more details about this issue, see Ref. [22].

IV. *NN* SCATTERING IN PERIPHERAL PARTIAL WAVES

In this section, we will calculate the phase shifts that result from the NN amplitudes presented in the previous section and compare them to the empirical phase shifts as well as to the predictions from conventional meson theory. For this comparison to be realistic, we must also include the one-pion-exchange amplitude and the iterated one-pion exchange, which we will explain first. We then describe in detail how the phase shifts are calculated. Finally, we show phase parameters for F and higher partial waves and energies below 300 MeV.

A. OPE and iterated OPE

Throughout this paper, we consider neutron-proton (np) scattering and take the charge dependence of OPE due to pion-mass splitting into account, since it is appreciable. Introducing the definition

$$V_\pi(m_\pi) \equiv -\frac{1}{(2\pi)^3}\frac{g_A^2}{4f_\pi^2}\frac{\vec{\sigma}_1\cdot\vec{q}\,\vec{\sigma}_2\cdot\vec{q}}{q^2+m_\pi^2}, \tag{62}$$

the charge-dependent OPE for np scattering is given by

$$V_{\rm OPE}(\vec{p}',\vec{p}) = -V_\pi(m_{\pi^0}) + (-1)^{I+1}2V_\pi(m_{\pi^\pm}), \tag{63}$$

where I denotes the isospin of the two-nucleon system. We use $m_{\pi^0}=134.9766$ MeV and $m_{\pi^\pm}=139.5702$ MeV [26].

The twice-iterated OPE generates the iterative part of the 2π exchange, which is

$$V_{2\pi,it}(\vec{p}',\vec{p}) = \frac{M_N^2}{E_p}\int d^3p'' \frac{V_{\rm OPE}(\vec{p}',\vec{p}'')V_{\rm OPE}(\vec{p}'',\vec{p})}{p^2-p''^2+i\epsilon}, \tag{64}$$

where, for M_N, we use twice the reduced mass of the proton and neutron,

$$M_N = \frac{2M_pM_n}{M_p+M_n} = 938.9182 \text{ MeV}, \tag{65}$$

and $E_p \equiv \sqrt{M_N^2+p^2}$.

The T matrix considered in this study is

$$T(\vec{p}',\vec{p}) = V_{\rm OPE}(\vec{p}',\vec{p}) + V_{2\pi,it}(\vec{p}',\vec{p}) + V_{2\pi,irr}(\vec{p}',\vec{p}), \tag{66}$$

where $V_{2\pi,irr}$ refers to any or all of the contributions presented in Sec. III. In the calculation of the latter contributions, we use the average pion mass $m_\pi=138.039$ MeV and, thus, neglect the charge dependence due to pion-mass splitting. The charge dependence that emerges from irreducible 2π exchange was investigated in Ref. [29] and found to be negligible for partial waves with $L \geqslant 3$.

B. Calculating phase shifts

We perform a partial-wave decomposition of the amplitude using the formalism of Refs. [30–32]. For this purpose, we first represent $T(\vec{p}',\vec{p})$, Eq. (66), in terms of helicity states yielding $\langle \vec{p}'\lambda_1'\lambda_2'|T|\vec{p}\lambda_1\lambda_2\rangle$. Note that the helicity λ_i of particle i (with $i=1$ or 2) is the eigenvalue of the helicity operator $\frac{1}{2}\vec{\sigma}_i\cdot\vec{p}_i/|\vec{p}_i|$ which is $\pm\frac{1}{2}$. Decomposition into angular momentum states is accomplished by

$$\begin{aligned}\langle \lambda_1'\lambda_2'|T^J(p',p)|\lambda_1\lambda_2\rangle &= 2\pi\int_{-1}^{+1} d(\cos\theta) d^J_{\lambda_1-\lambda_2,\lambda_1'-\lambda_2'}(\theta) \\ &\times \langle \vec{p}'\lambda_1'\lambda_2'|T|\vec{p}\lambda_1\lambda_2\rangle,\end{aligned} \tag{67}$$

where θ is the angle between $\vec{p}'$ and $\vec{p}$ and $d^J_{m,m'}(\theta)$ are the conventional reduced rotation matrices which can be expressed in terms of Legendre polynominals $P_J(\cos\theta)$. Time-reversal invariance, parity conservation, and spin conservation (which is a consequence of isospin, conservation and the Pauli principle) imply that only five of the 16 helicity amplitudes are independent. For the five amplitudes, we choose the following set:

$$\begin{aligned} T_1^J(p,p) &\equiv \langle ++|T^J(p,p)|++\rangle, \\ T_2^J(p,p) &\equiv \langle ++|T^J(p,p)|--\rangle, \\ T_3^J(p,p) &\equiv \langle +-|T^J(p,p)|+-\rangle, \\ T_4^J(p,p) &\equiv \langle +-|T^J(p,p)|-+\rangle, \\ T_5^J(p,p) &\equiv \langle ++|T^J(p,p)|+-\rangle, \end{aligned} \tag{68}$$

where $\pm$ stands for $\pm\frac{1}{2}$ and where the repeated argument (p,p) stresses the fact that our consideration is restricted to the on-shell amplitude. The following linear combinations of helicity amplitudes will prove to be useful:

$$\begin{aligned} {}^0T^J &\equiv T_1^J - T_2^J, \\ {}^1T^J &\equiv T_3^J - T_4^J, \\ {}^{12}T^J &\equiv T_1^J + T_2^J, \\ {}^{34}T^J &\equiv T_3^J + T_4^J, \\ {}^{55}T^J &\equiv 2T_5^J. \end{aligned} \tag{69}$$

More common in nuclear physics is the representation of two-nucleon states in terms of an $|LSJM\rangle$ basis, where S denotes the total spin, L the total orbital angular momentum, and J the total angular momentum with projection M. In this basis, we will denote the T-matrix elements by $T^{JS}_{L',L} \equiv \langle L'SJM|T|LSJM\rangle$. These are obtained from the helicity state matrix elements by the following unitary transformation:

Spin singlet

$$T^{J0}_{J,J} = {}^0T^J. \tag{70}$$

Uncoupled spin triplet

$$T^{J1}_{J,J} = {}^1T^J. \tag{71}$$

Coupled triplet states

$$\begin{aligned} T^{J1}_{J-1,J-1} &= \frac{1}{2J+1}[J\,{}^{12}T^J + (J+1)\,{}^{34}T^J + 2\sqrt{J(J+1)}\,{}^{55}T^J], \\ T^{J1}_{J+1,J+1} &= \frac{1}{2J+1}[(J+1)\,{}^{12}T^J + J\,{}^{34}T^J - 2\sqrt{J(J+1)}\,{}^{55}T^J], \\ T^{J1}_{J-1,J+1} &= \frac{1}{2J+1}[\sqrt{J(J+1)}({}^{12}T^J - {}^{34}T^J) + {}^{55}T^J], \\ T^{J1}_{J+1,J-1} &= T^{J1}_{J-1,J+1}. \end{aligned} \tag{72}$$

The matrix elements for the five spin-dependent operators involved in Eq. (16) in a helicity state basis, Eqs. (67), as

well as in $|LSJM\rangle$ basis, Eq. (72), are given in Sec. IV of Ref. [32]. Note that, for the amplitudes $T^{J1}_{J-1,J+1}$ and $T^{J1}_{J+1,J-1}$, we use a sign convention that differs by a factor (-1) from the one used in Ref. [32].

We consider neutron-proton scattering and determine the c.m. on-shell nucleon momentum p using the correct relativistic kinematics:

$$p^2=\frac{M_p^2 T_{lab}(T_{lab}+2M_n)}{(M_p+M_n)^2+2T_{lab}M_p}, \tag{73}$$

where $M_p=938.2720$ MeV is the proton mass, $M_n=939.5653$ MeV the neutron mass [26], and T_{lab} the kinetic energy of the incident nucleon in the laboratory system.

The on-shell S matrix is related to the on-shell T matrix by

$$S^{JS}_{L'L}(T_{lab})=\delta_{L'L}+2i\,\tau^{JS}_{L'L}(p,p), \tag{74}$$

with

$$\tau^{JS}_{L'L}(p,p)\equiv-\frac{\pi}{2}\frac{M_N^2}{E_p}pT^{JS}_{L'L}(p,p). \tag{75}$$

For an uncoupled partial wave, the phase shifts $\delta^{JS}_J(T_{lab})$ parametrizes the partial-wave S matrix in the form

$$S^{JS}_{JJ}(T_{lab})=\eta^{JS}_J(T_{lab})e^{2i\delta^{JS}_J(T_{lab})}, \tag{76}$$

implying

$$\tan 2\,\delta^{JS}_J(T_{lab})=\frac{2\,\mathrm{Re}\,\tau^{JS}_{JJ}(p,p)}{1-2\,\mathrm{Im}\,\tau^{JS}_{JJ}(p,p)}. \tag{77}$$

The real parameter $\eta^{JS}_J(T_{lab})$, which is given by

$$\eta^{JS}_J(T_{lab})=|S^{JS}_{JJ}(T_{lab})|, \tag{78}$$

tells us to what extent unitarity is observed (ideally, it should be unity).

For coupled partial waves, we use the parametrization introduced by Stapp *et al.* [33] (commonly known as "bar" phase shifts, *but we denote them simply by* $\delta^J_\pm$ *and* ϵ_J):

$$\begin{pmatrix} S^J_{--} & S^J_{-+} \\ S^J_{+-} & S^J_{++} \end{pmatrix} = \begin{pmatrix} (\eta^J_-)^{1/2}e^{i\delta^J_-} & 0 \\ 0 & (\eta^J_+)^{1/2}e^{i\delta^J_+} \end{pmatrix} \begin{pmatrix} \cos 2\epsilon_J & i\sin 2\epsilon_J \\ i\sin 2\epsilon_J & \cos 2\epsilon_J \end{pmatrix} \times \begin{pmatrix} (\eta^J_-)^{1/2}e^{i\delta^J_-} & 0 \\ 0 & (\eta^J_+)^{1/2}e^{i\delta^J_+} \end{pmatrix}, \tag{79}$$

where the subscript "+" stands for "$J+1$" and "$-$" for "$J-1$" and where the superscript $S=1$ as well as the argument T_{lab} are suppressed. The explicit formulas for the resulting phase parameters are

$$\tan 2\,\delta^J_\pm=\frac{\mathrm{Im}(S^J_{\pm\pm}/\cos 2\epsilon_J)}{\mathrm{Re}(S^J_{\pm\pm}/\cos 2\epsilon_J)}, \tag{80}$$

$$\tan 2\,\epsilon_J=\frac{-iS^J_{+-}}{\sqrt{S^J_{++}S^J_{--}}}, \tag{81}$$

$$\eta^J_\pm=\left|\frac{S^J_{\pm\pm}}{\cos 2\epsilon_J}\right|. \tag{82}$$

The parameters $\delta^J_\pm$ and $\eta^J_\pm$ are always real, while the mixing parameter ϵ_J is real if $\eta^J_\pm=1$ and complex otherwise.

We note that since the T matrix is calculated perturbatively [cf. Eq. (66)], unitarity is (slightly) violated. Through the parameter η^{JS}_L, the above formalism provides precise information on the violation of unitarity. It turns out that for the cases considered in this paper (namely partial waves with $L\geqslant 3$ and $T_{lab}\leqslant 300$ MeV) the violation of unitarity is, generally, of the order of 1% or less.

There exists an alternative method of calculating phase shifts for which unitarity is perfectly observed. In this method—known as the K-matrix approach—one identifies the real part of the amplitude V with the K matrix. For an uncoupled partial wave, the S-matrix element S_L is defined in terms of the (real) K-matrix element κ_L by

$$S_L(T_{lab})=\frac{1+i\kappa_L(p,p)}{1-i\kappa_L(p,p)}, \tag{83}$$

which guarantees perfect unitarity and yields the phase shift

$$\tan\delta_L(T_{lab})=\kappa_L(p,p)=-\frac{\pi}{2}\frac{M_N^2}{E_p}pK_L(p,p), \tag{84}$$

with $K_L(p,p)=\mathrm{Re}\,V_L(p,p)$. Combining Eqs. (74) and (83), one can write down the T-matrix element τ_L, which is equivalent to a given K-matrix element κ_L,

$$\tau_L(p,p)=\frac{\kappa_L(p,p)+i\kappa_L^2(p,p)}{1+\kappa_L^2(p,p)}. \tag{85}$$

Obviously, this T matrix includes higher orders of K (and, thus, of V) such that consistent power counting is destroyed.

The bottom line is that there is no perfect way of calculating phase shifts for a perturbative amplitude. Either one includes contributions strictly to a certain order, but violates unitarity, or one satisfies unitarity, but includes implicitly contributions beyond the intended order. To obtain an idea of what uncertainty this dilemma creates, we have calculated all phase shifts presented below both ways: using the T-matrix and K-matrix approaches. We found that the difference between the phase shifts due to the two different methods is smaller than 0.1° in F and G waves and smaller than 0.01° in H waves, at $T_{\mathrm{lab}}=300$ MeV (and less at lower energies). Because of this small difference, we have confidence in our phase shift calculations. All results presented below have been obtained using the T-matrix approach, Eqs. (74)–(82).

C. Results

For the T matrix given in Eq. (66), we calculate phase shifts for partial waves with $L \geqslant 3$ and $T_{lab} \leqslant 300$ MeV. At fourth order in small momenta, partial waves with $L \geqslant 3$ do not receive any contributions from contact interactions and, thus, the nonpolynomial pion contributions uniquely predict the F and higher partial waves. The parameters used in our calculations are shown in Table I. In general, we use average masses for the nucleon and pion, M_N and m_π, as given in Table I. There are, however, two exceptions to this rule. For the evaluation of the c.m. on-shell momentum p, we apply correct relativistic kinematics, Eq. (73), which involves the correct and precise values for the proton and neutron masses. For OPE, we use the charge-dependent expression, Eq. (63), which employs the correct and precise values for the charged and neutral pion masses.

Many determinations of the LECs c_i and $\overline{d_i}$ can be found in the literature. The most reliable way to determine the LECs from empirical πN information is to extract them from the πN amplitude inside the Mandelstam triangle (unphysical region) which can be constructed with the help of dispersion relations from empirical πN data. This method was used by Büttiker and Meißner [27]. Unfortunately, the values for c_2 and all $\overline{d_i}$ parameters obtained in Ref. [27] carry uncertainties so large that the values are useless. Therefore, in Table I, only c_1, c_3, and c_4 are from Ref. [27], while the other LECs are taken from Ref. [22] where the πN amplitude in the physical region was considered. To establish a link between πN and NN, we apply the values from the above determinations in our NN calculations. In general, we use the mean values; the only exception is c_3, where we choose a value that is, in terms of magnitude, about one standard deviation below the one from Ref. [27]. With the exception of c_3, our results do not depend sensitively on variations of the LECs within the quoted uncertainties.

In Figs. 4–6, we show the phase-shift predictions for neutron-proton scattering in F, G, and H waves for laboratory kinetic energies below 300 MeV. The orders displayed are defined as follows.

(i) Leading order (LO) is just OPE, Eq. (63).

(ii) Next-to-leading order (NLO) is OPE plus iterated OPE, Eq. (64), plus the contributions of Sec. III A (second order), Eqs. (17) and (18).

(iii) Next-to-next-to-leading order (denoted by N2LO in the figures) consists of NLO plus the contributions of Sec. III.B (third order), Eqs. (21)–(26).

(iv) Next-to-next-to-next-to-leading order (denoted by N3LO in the figures) consists of N2LO plus the contributions of Sec. III C (fourth order), Eqs. (29), (30), (31)–(35), (36)–(42), and (54)–(61). To this order, the phase shifts have never been calculated before.

It is clearly seen in Figs. 4–6 that the leading order 2π exchange (NLO) is a rather small contribution, insufficient to explain the empirical facts. In contrast, the next order (N2LO) is very large, several times NLO. This is due to the $\pi\pi NN$ contact interactions proportional to the LECs c_i that are introduced by the second order Lagrangian $\mathcal{L}^{(2)}_{\pi N}$, Eq. (9). These contacts are supposed to simulate the contributions from intermediate Δ isobars and correlated 2π exchange which are known to be large (see, e.g., Ref. [36]).

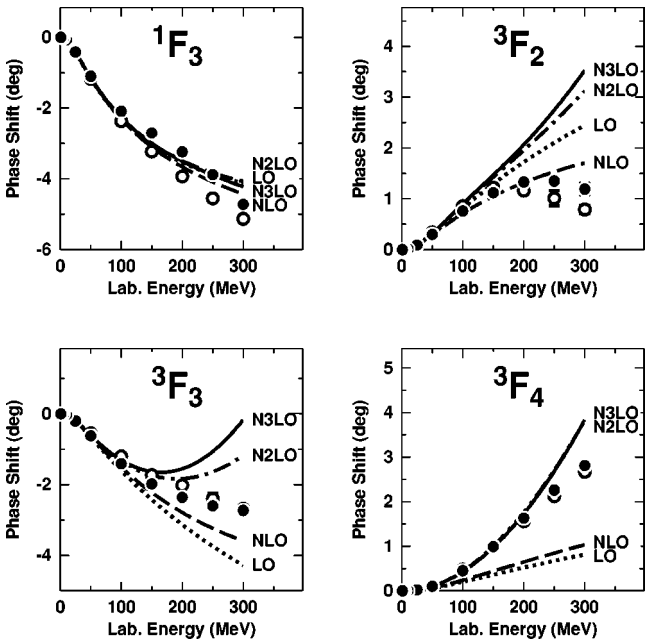

FIG. 4. F-wave phase shifts of neutron-proton scattering for laboratory kinetic energies below 300 MeV. We show the predictions from chiral pion exchange to leading order (LO), next-to-leading order (NLO), next-to-next-to-leading order (N2LO), and next-to-next-to-next-to-leading order (N3LO). The solid dots and open circles are the results from the Nijmegen multienergy np phase shift analysis [34] and the Virginia Polytechnic Institute single-energy np analysis SM99 [35], respectively.

All past calculations of NN phase shifts in peripheral partial waves stopped at order N2LO (or lower). This was very unsatisfactory, since to this order there is no indication that

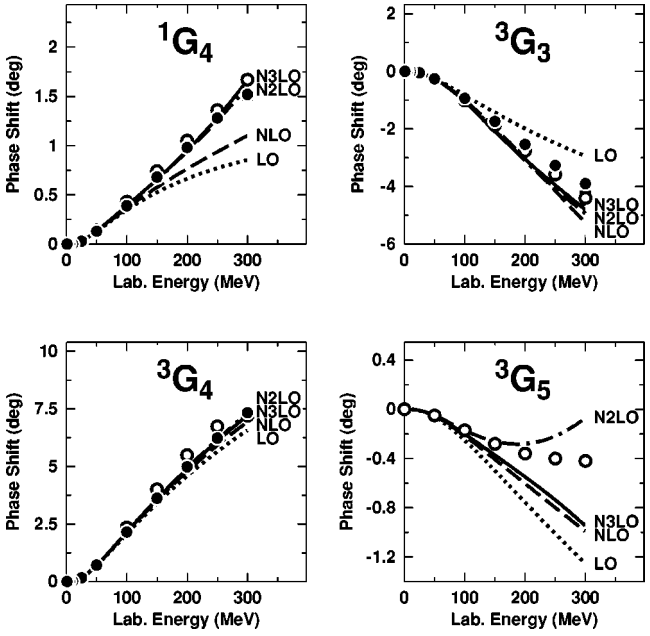

FIG. 5. Same as Fig. 4, but for G waves.

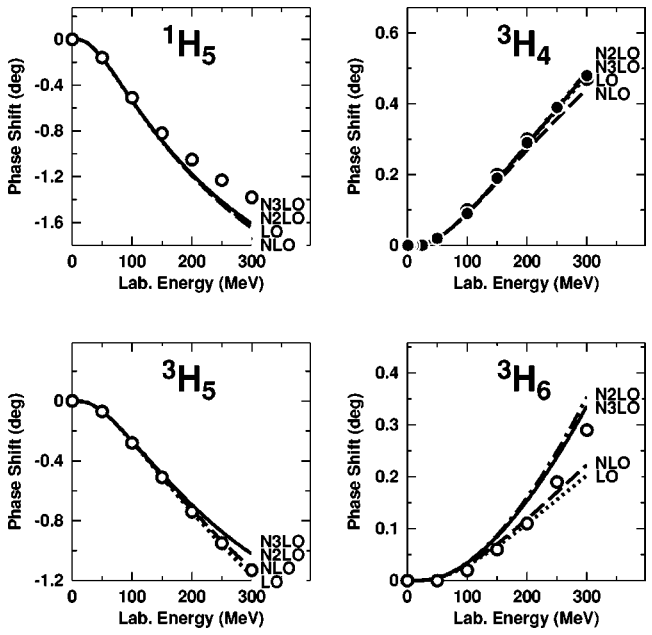

FIG. 6. Same as Fig. 4, but for H waves.

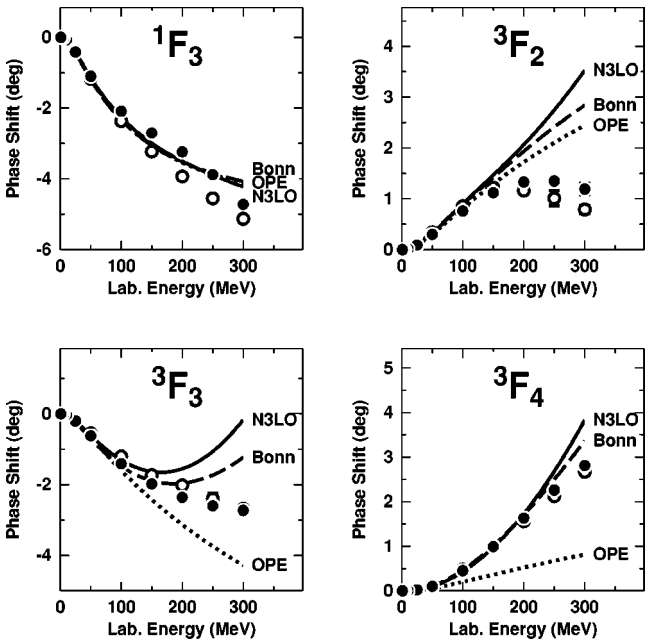

FIG. 7. F-wave phase shifts of neutron-proton scattering for laboratory kinetic energies below 300 MeV. We show the results from one-pion exchange (OPE) and one- plus two-pion exchange as predicted by χPT at next-to-next-to-next-to-leading order (N3LO) and by the Bonn full model [36] (Bonn). Empirical phase shifts (solid dots and open circles) as in Fig. 4.

the chiral expansion will ever converge. The novelty of the present work is the calculation of phase shifts to N3LO (the details of which are shown in the Appendix). Comparison with N2LO reveals that at N3LO a clearly identifiable trend towards convergence emerges (Figs. 4–6). In G (except for $^3G_5$, a problem that is discussed in the Appendix) and H waves, N3LO differs very little from N2LO, implying that we have reached convergence. Also $^1F_3$ and $^3F_4$ appear fully converged. In $^3F_2$ and $^3F_3$, N3LO differs noticeably from N2LO, but the difference is much smaller than the one between N2LO and NLO. This is what we perceive as a trend towards convergence.

In Figs. 7–9, we conduct a comparison between the predictions from chiral one- and two-pion exchange at N3LO and the corresponding predictions from conventional meson theory (curve "Bonn"). As representative for conventional meson theory, we choose the Bonn meson-exchange model for the NN interaction [36], since it contains a comprehensive and thoughtfully constructed model for 2π exchange. This 2π model includes box and crossed box diagrams with NN, $N\Delta$, and $\Delta\Delta$ intermediate states as well as direct $\pi\pi$ interaction in S and P waves (of the $\pi\pi$ system) consistent with empirical information from πN and $\pi\pi$ scattering. Besides this the Bonn model also includes (repulsive) ω-meson exchange and irreducible diagrams of π and ρ exchange (which are also repulsive). In the phase-shift predictions displayed in Figs. 7–9, the Bonn calculation includes only the OPE and 2π contributions from the Bonn model; the short-range contributions are left out to be consistent with the chiral calculation. In all waves shown (with the usual exception of $^3G_5$), we see, in general, good agreement between N3LO and Bonn [37]. In $^3F_2$ and $^3F_3$ above 150 MeV and in $^3F_4$ above 250 MeV the chiral model to N3LO is more attractive than the Bonn 2π model. Note, however, that the Bonn model is relativistic and, thus, includes relativistic corrections up to infinite orders. Thus, one may speculate that higher orders in chiral perturbation theory (χPT) may create some repulsion, moving the Bonn and the chiral predictions even closer together [38].

The 2π-exchange contribution to the NN interaction can also be derived from *empirical* πN and $\pi\pi$ input using dispersion theory, which is based upon unitarity, causality (analyticity), and crossing symmetry. The amplitude $N\bar{N}\to\pi\pi$ is

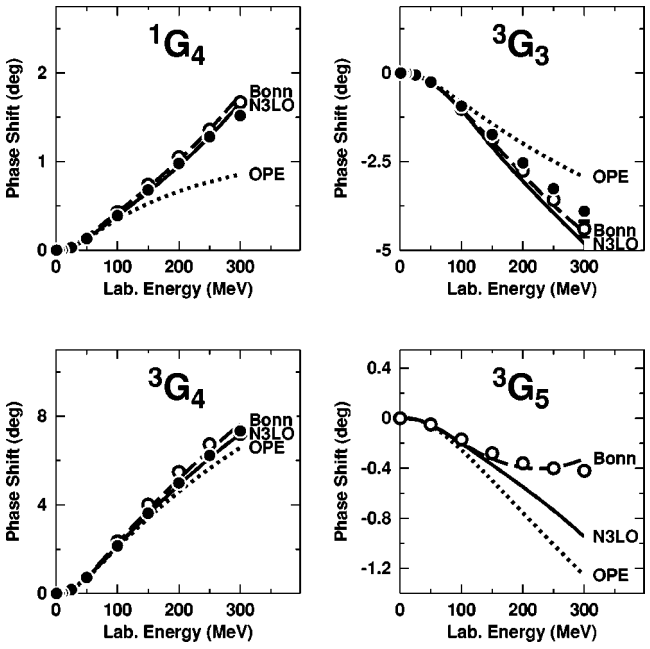

FIG. 8. Same as Fig. 7, but for G waves.

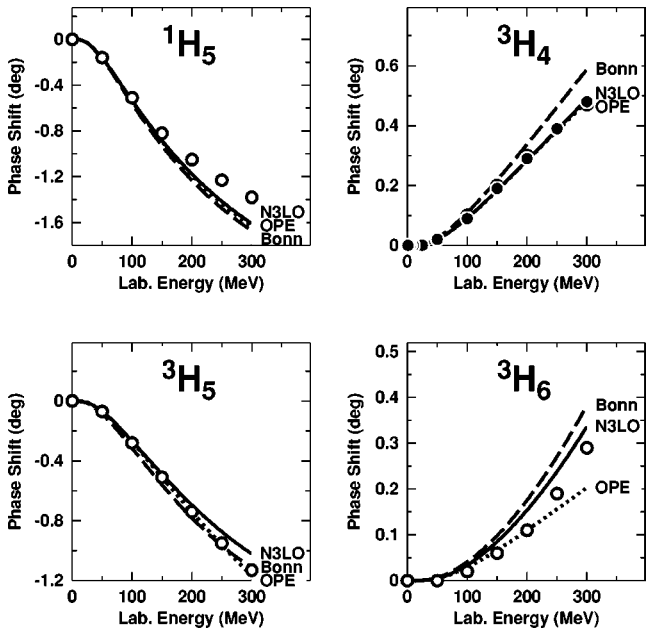

FIG. 9. Same as Fig. 7, but for H waves.

constructed from $\pi N \to \pi N$ and $\pi N \to \pi\pi N$ data using crossing properties and analytic continuation; this amplitude is then ''squared'' to yield the $N\bar{N}$ amplitude which is related to NN by crossing symmetry [39]. The Paris group [40] pursued this path and calculated NN phase shifts in peripheral partial waves. Naively, the dispersion-theoretic approach is the ideal one, since it is based exclusively on empirical information. Unfortunately, in practice, quite a few uncertainties enter into the approach. First, there are ambiguities in the analytic continuation and, second, the dispersion integrals have to be cut off at a certain momentum to ensure reasonable results. In Ref. [36], a thorough comparison was conducted between the predictions by the Bonn model and the Paris approach and it was demonstrated that the Bonn predictions always lie comfortably within the range of uncertainty of the dispersion-theoretic results. Therefore, there is no need to perform a separate comparison of our chiral N3LO predictions with dispersion theory, since it would not add anything that we cannot conclude from Figs. 7–9.

Finally, we like to compare the predictions with the empirical phase shifts. In G (except $^3G_5$) and H waves there is excellent agreement between the N3LO predictions and the data. On the other hand, in F waves the predictions above 200 MeV are, in general, too attractive. Note, however, that this is also true for the predictions by the Bonn $\pi+2\pi$ model. In the full Bonn model, also (repulsive) ω and $\pi\rho$ exchanges are included which bring the predictions to agreement with the data. The exchange of a ω meson or combined $\pi\rho$ exchange are 3π exchanges. Three-pion exchange occurs first at chiral fourth order. It has be investigated by Kaiser [9] and found to be totally negligible, at this order. However, 3π exchange at fifth order appears to be sizable [10] and may have an impact on F waves. Besides this, there is the usual short-range phenomenology. In χPT, this short-range interaction is parametrized in terms of four-nucleon contact terms (since heavy mesons do not have a place in that theory). Contact terms of sixth order are effective in F waves. In summary, the remaining small discrepancies between the N3LO predictions and the empirical phase shifts may be straightened out in fifth or sixth order of χPT.

V. CONCLUSIONS AND FURTHER DISCUSSION

We have calculated the phase shifts for peripheral partial waves ($L \geqslant 3$) of neutron-proton scattering at fourth order (N^3LO) in χPT. The two most important conclusions from this study are the following.

(i) At N^3LO, the chiral expansion reveals a clearly identifiable signature of convergence.

(ii) There is good agreement between the N^3LO prediction and the corresponding one from conventional meson theory as represented by the Bonn full model [36].

Besides the above fundamentally important statements, our study has also some more specific implications. A controversial issue that has recently drawn a lot of attention [41] is the question whether the LECs extracted from πN are consistent with NN. After discussing dispersion theory in the previous section, one may wonder how this can be an issue in the year of 2002. In the early 1970s, the Stony Brook [42,39] and the Paris [43,40] groups showed independently that πN and NN are consistent, based upon dispersion-theoretic calculations. Since dispersion theory is a model-independent approach, the finding is of general validity. Therefore, if 30 years later a specific theory has problems with the consistency of πN and NN, then that theory can only be wrong. Fortunately, we can confirm that χPT for πN and NN does yield consistent results, as we will explain now in more detail.

The reliable way to investigate this issue is to use an approach that does not contain any parameters except for the LECs. This is exactly true for our calculations since we do not use any cutoffs and calculate the T matrix directly up to a well-defined order. We then vary the LECs within their one-standard-deviation range from the πN determinations (cf. Table I). We find that these variations do not create any essential changes of the predicted peripheral NN phase shifts shown in Figs. 4–9, except for c_3. Thus, the focus is on c_3. We find that $c_3 = -3.4$ GeV^{-1} is consistent with the empirical phase shifts as well as the results from dispersion theory and conventional meson theory as demonstrated in Figs. 7–9. This choice for c_3 is within one standard deviation of its πN determination and, thus, the consistency of πN and NN in χPT at fourth order is established.

In view of the transparent and conclusive consideration presented above, it is highly disturbing to find in the literature very different values for c_3, allegedly based upon NN. In Ref. [21], it its claimed that the value $c_3 = -5.08 \pm 0.28$ GeV^{-1} emerges from the world pp data below 350 MeV, whereas Ref. [41] asserts that $c_3 = -1.15$ GeV^{-1} is implied by the NN phase shifts. The two values differ by more than 400% which is reason for deep concern.

In Fig. 10, we show the predictions at fourth order for the three values for c_3 under debate. We have chosen $^3F_4$ as a representative example of a peripheral partial wave since it has a rather large contribution from 2π exchange. Moreover,

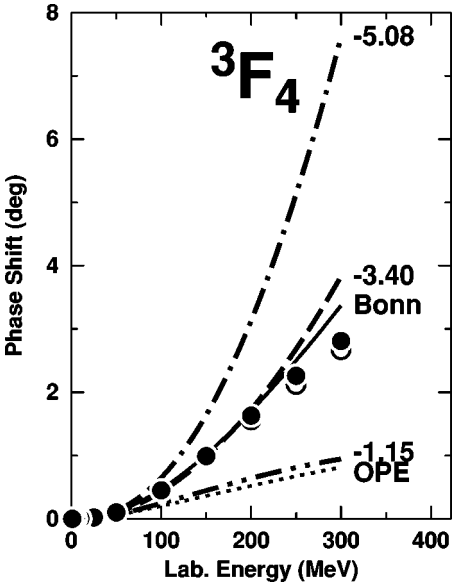

FIG. 10. One- and two-pion-exchange contributions at fourth order to the $^3F_4$ phase shifts for three different choices of the LEC c_3. The numbers given next to the curves denote the values for c_3 in units of GeV^{-1} used for the respective curves (all other parameters as in Table I). For comparison, we also show the OPE contributrion (OPE) and the result from $\pi+2\pi$ exchange of the Bonn model (Bonn). Empirical phase shifts (solid dots and open circles) as in Fig. 4.

the LEC c_4 is ineffective in $^3F_4$ such that differences in the choices for c_4 do not distort the picture in this partial wave. This fact makes $^3F_4$ special for the discussion of c_3.

Figure 10 reveals that the chiral 2π exchange depends most sensitively on c_3. It is clearly seen that the Nijmegen choice $c_3=-5.08\ \mathrm{GeV}^{-1}$ [21] leads to too much attraction, while the value $c_3=-1.15\ \mathrm{GeV}^{-1}$, advocated in Ref. [41], is far too small (in terms of magnitude) since it results in an almost vanishing 2π-exchange contribution—quite in contrast to the empirical *NN* facts, the dispersion-theoretic result, and the Bonn model.

One reason for the difference between the Nijmegen value and ours could be that their analysis is conducted at $\mathrm{N^2LO}$, while we go to $\mathrm{N^3LO}$. However, as demonstrated in Figs. 4–6, $\mathrm{N^3LO}$ is not that different from $\mathrm{N^2LO}$ and, therefore, not the main reason for the difference. More crucial is the fact that, in the Nijmegen analysis, the chiral 2π-exchange potential, represented as a local *r*-space function, is cut off at $r=1.4$ fm (i.e., it is set to zero for $r\leqslant 1.4$ fm) [44]. This cutoff suppresses the 2π contribution, also, in peripheral waves. If the 2π potential is suppressed by phenomenology, then, of course, stronger values for c_3 are necessary, resulting in a highly model-dependent determination of c_3. For example, if we multiply all noniterative 2π contributions by $\exp[-(p^{2n}+p'^{\,2n})/\Lambda^{2n}]$ with $\Lambda\approx 400$ MeV and $n=2$, then with $c_3=-5.08\ \mathrm{GeV}^{-1}$ we obtain a good reproduction of the peripheral partial-wave phase shifts. Note that $\Lambda\approx 400$ MeV is roughly equivalent to a *r*-space cutoff of about 0.5 fm, which is not even close to the cutoff used in the Nijmegen analysis. In fact, the Nijmegen *r*-space cutoff of $r=1.4$ fm is equivalent to a momentum-space cutoff $\Lambda\approx m_\pi$ which is bound to kill the 2π exchange contribution (which has a momentum-space range of $2m_\pi$ and larger). To revive it, unrealistically large parameters are necessary.

The motivation underlying the value for c_3 advocated in Ref. [41] is quite different from the Nijmegen scenario. In Ref. [41], c_3 was adjusted to the *D* waves of *NN* scattering, which are notoriously too attractive. With their choice $c_3=-1.15\ \mathrm{GeV}^{-1}$, the *D* waves are, indeed, about right, whereas the *F* waves are drastically underpredicted. This violates an important rule: *The higher the partial, the higher the priority*. The reason for this rule is that we have more trust in the long-range contributions to the nuclear force than in the short-range ones. The $\pi+2\pi$ contributions to the nuclear force rule the *F* and higher partial waves, not the *D* waves. If *D* waves do not come out right, then one can think of plenty of short-range contributions to fix it. If *F* and higher partial waves are wrong, there is no fix.

In summary, a realistic choice for the important LEC c_3 is $-3.4\ \mathrm{GeV}^{-1}$ and one may deliberately assign an uncertainty of $\pm 10\%$ to this value. Substantially different values are unrealistic as clearly demonstrated in Fig. 10.

ACKNOWLEDGMENTS

We would like to thank N. Kaiser for substantial advice throughout this project. Interesting communications with J. W. Durso are gratefully acknowledged. This work was supported in part by the U.S. National Science Foundation under Grant No. PHY-0099444 and by the Ramón Areces Foundation (Spain).

APPENDIX: DETAILS OF FOURTH-ORDER CONTRIBUTIONS TO PERIPHERAL PARTIAL-WAVE PHASE SHIFTS

The fourth order consists of very many contributions (cf. Sec. III C and Figs. 2 and 3). Here, we show how the various contributions of fourth order impact *NN* phase shifts in peripheral partial waves. For this purpose, we display in Fig. 11 phase shifts for four important peripheral partial waves: namely, $^1F_3$, $^3F_3$, $^3F_4$, and $^3G_5$. In each frame, the following individual fourth-order contributions are shown.

(i) c_i^2 graph, first row of Fig. 2, Eqs. (29) and (30), denoted by "c2" in Fig. 11.

(ii) c_i/M_N contributions (denoted by "c/M"), second row of Fig. 2, Eqs. (31)–(35).

(iii) $1/M_n^2$ corrections ("1/M2"), rows 3–6 of Fig. 2, Eqs. (36)–(42).

(iv) Two-loop contributions without the terms proportional to $\overline{d_i}$ ("2-L"): Fig. 3, but without the solid square, Eqs. (54)–(61), but with all $\overline{d_i}\equiv 0$.

(v) Two-loop contributions including the terms proportional to $\overline{d_i}$ (denoted by "d" in Fig. 11): Fig. 3, Eqs. (54)–(61) with the $\overline{d_i}$ parameters as given in Table I.

Starting with the result at N2LO, curve (1), the individual N3LO contributions are added up successively in the order

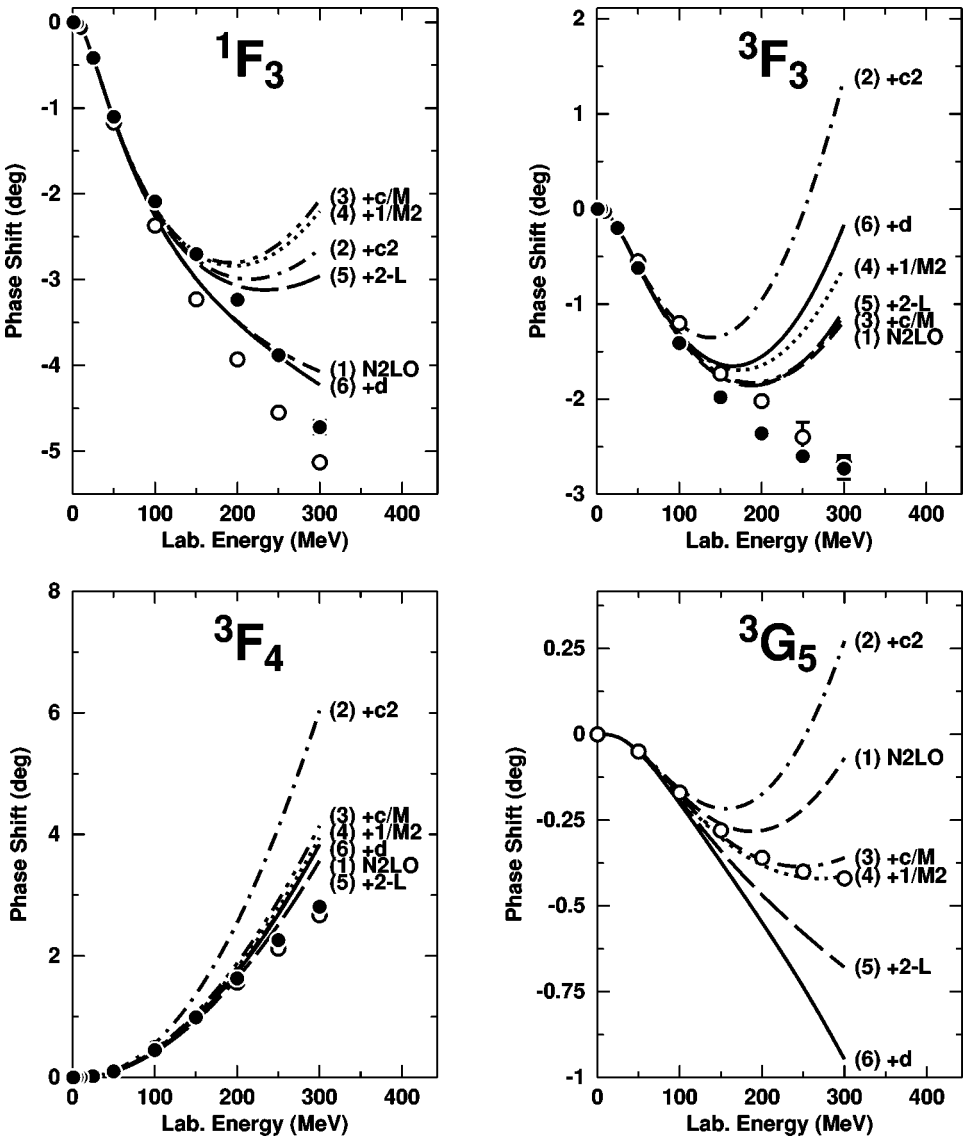

FIG. 11. The effect of individual fourth-order contributions on the neutron-proton phase shifts in some selected peripheral partial waves. The individual contributions are added up successively in the order given in parentheses next to each curve. Curve (1) is N2LO and curve (6) is the complete N3LO. For further explanations, see the Appendix. Empirical phase shifts (solid dots and open circles) as in Fig. 4.

given in parentheses next to each curve. The last curve in this series, curve (6), is the full N3LO result.

The c_i^2 graph generates large attraction in all partial waves [cf. differences between curves (1) and (2) in Fig. 11]. This attraction is compensated by repulsion from the c_i/M_N diagrams, in most partial waves; the exception is $^1F_3$ where c_i/M_N adds more attraction [curve (3)]. The $1/M_N^2$ corrections [difference between curves (3) and (4)] are typically small. Finally, the two-loop contributions create substantial repulsion in $^1F_3$ and $^3G_5$ which brings $^1F_3$ into good agreement with the data while causing a discrepancy for $^3G_5$. In $^3F_3$ and $^3F_4$, there are large cancellations between the ''pure'' two-loop graphs and the $\overline{d}_i$ terms, making the net two-loop contribution rather small.

A pivotal role in the above game is played by W_S, Eq. (33), from the c_i/M_N group. This attractive term receives a factor of 9 in $^1F_3$, a factor (-3) in $^3G_5$ and a factor of 1 in $^3F_3$ and $^3F_4$. Thus, this contribution is very attractive in $^1F_3$ and repulsive in $^3G_5$. The latter is the reason for the overcompensation of the c_i^2 graph by the c_i/M_N contribution in $^3G_5$ which is why the final N3LO result in this partial wave comes out too repulsive. One can expect that $1/M_N$ corrections that occur at fifth or sixth order will resolve this problem.

Before finishing this appendix, we like to point out that the problem with the $^3G_5$ is not as dramatic as it may appear from the phase-shift plots—for two reasons. First, the $^3G_5$ phase shifts are about one order of magnitude smaller than the F and most of the other G phases. Thus, in absolute terms, the discrepancies seen in $^3G_5$ are small. In a certain sense, we are looking at ''higher-order noise'' under a magnifying glass. Second, the $^3G_5$ partial wave contributes 0.06 MeV to the energy per nucleon in nuclear matter, the total of which is -16 MeV. Consequently, small discrepancies in the reproduction of $^3G_5$ by a NN interaction model will have negligible influence on the microscopic nuclear structure predictions obtained with that model.

[1] S. Weinberg, Phys. Lett. B **251**, 288 (1990); Nucl. Phys. **B363**, 3 (1991).
[2] C. Ordóñez and U. van Kolck, Phys. Lett. B **291**, 459 (1992).
[3] C. Ordóñez, L. Ray, and U. van Kolck, Phys. Rev. Lett. **72**, 1982 (1994); Phys. Rev. C **53**, 2086 (1996).
[4] U. van Kolck, Prog. Part. Nucl. Phys. **43**, 337 (1999).
[5] L. S. Celenza, A. Pantziris, and C. M. Shakin, Phys. Rev. C **46**, 2213 (1992).
[6] C. A. da Rocha and M. R. Robilotta, Phys. Rev. C **49**, 1818 (1994); **52**, 531 (1995); M. R. Robilotta, Nucl. Phys. **A595**, 171 (1995); M. R. Robilotta and C. A. da Rocha, *ibid.* **A615**, 391 (1997); J.-L. Ballot, C. A. da Rocha, and M. R. Robilotta, Phys. Rev. C **57**, 1574 (1998).
[7] N. Kaiser, R. Brockmann, and W. Weise, Nucl. Phys. **A625**, 758 (1997).
[8] N. Kaiser, S. Gerstendörfer, and W. Weise, Nucl. Phys. **A637**, 395 (1998).
[9] N. Kaiser, Phys. Rev. C **61**, 014003 (1999); **62**, 024001 (2000).
[10] N. Kaiser, Phys. Rev. C **63**, 044010 (2001).
[11] N. Kaiser, Phys. Rev. C **64**, 057001 (2001).
[12] N. Kaiser, Phys. Rev. C **65**, 017001 (2002).
[13] E. Epelbaum, W. Glöckle, and U.-G. Meißner, Nucl. Phys. **A637**, 107 (1998); **A671**, 295 (2000).
[14] D. R. Entem and R. Machleidt, Phys. Lett. B **524**, 93 (2002).
[15] D. B. Kaplan, M. J. Savage, and M. B. Wise, Nucl. Phys. **B478**, 629 (1996); D. B. Kaplan, *ibid.* **B494**, 471 (1997); D. B. Kaplan, M. J. Savage, and M. B. Wise, *ibid.* **B534**, 329 (1998); Phys. Lett. B **424**, 390 (1998).
[16] R. J. Furnstahl, B. D. Serot, and H.-B. Tang, Nucl. Phys. **A615**, 441 (1997); J. V. Steel and R. J. Furnstahl, *ibid.* **A637**, 46 (1998); R. J. Furnstahl, J. V. Steel, and N. Tirfessa, *ibid.* **A671**, 396 (2000); R. J. Furnstahl, H. W. Hammer, and N. Tirfessa, *ibid.* **A689**, 846 (2001).
[17] T.-S. Park, K. Kubodera, D. P. Min, and M. Rho, Phys. Rev. C **58**, 637 (1998); Nucl. Phys. **A646**, 83 (1999).
[18] T. D. Cohen, Phys. Rev. C **55**, 67 (1997); D. R. Phillips and T. D. Cohen, Phys. Lett. B **390**, 7 (1997); K. A. Scaldeferri, D. R. Phillips, C. W. Kao, and T. D. Cohen, Phys. Rev. C **56**, 679 (1997); S. R. Beane, T. D. Cohen, and D. R. Phillips, Nucl. Phys. **A632**, 445 (1998).
[19] G. Rupak and N. Shoresh, nucl-th/9906077; P. F. Bedaque, H. W. Hammer, and U. van Kolck, Nucl. Phys. **A676**, 357 (2000); S. Fleming, Th. Mehen, and I. W. Stewart, *ibid.*, **A677**, 313 (2000); Phys. Rev. C **61**, 044005 (2000).
[20] S. R. Bean, P. F. Bedaque, M. J. Savage, and U. van Kolck, Nucl. Phys. **A700**, 377 (2002).
[21] M. C. M. Rentmeester, R. G. E. Timmermans, J. L. Friar, and J. J. de Swart, Phys. Rev. Lett. **82**, 4992 (1999).
[22] N. Fettes, U.-G. Meißner, and S. Steiniger, Nucl. Phys. **A640**, 199 (1998).
[23] N. Fettes, U.-G. Meißner, M. Mojžiš, and S. Steininger, Ann. Phys. (N.Y.) **283**, 273 (2000); **288**, 249 (2001).
[24] V. Stoks, R. Timmermans, and J. J. de Swart, Phys. Rev. C **47**, 512 (1993).
[25] R. A. Arndt, R. L. Workman, and M. M. Pavan, Phys. Rev. C **49**, 2729 (1994).
[26] Particle Data Group, D. E. Groom *et al.*, Eur. Phys. J. C **15**, 1 (2000).
[27] P. Büttiker and U.-G. Meißner, Nucl. Phys. **A668**, 97 (2000).
[28] V. Bernard, N. Kaiser, and U.-G. Meißner, Int. J. Mod. Phys. E **4**, 193 (1995).
[29] G. Q. Li and R. Machleidt, Phys. Rev. C **58**, 3153 (1998).
[30] M. Jacob and G. C. Wick, Ann. Phys. (N.Y.) **7**, 404 (1959).
[31] J. Goto and S. Machida, Prog. Theor. Phys. **25**, 64 (1961).
[32] K. Erkelenz, R. Alzetta, and K. Holinde, Nucl. Phys. **A176**, 413 (1971); note that there is an error in Eq. (4.22) of this paper where it should read

$$^{-}W^{J}_{LS}=2qq'\frac{J-1}{2J-1}[A^{J-2,(0)}_{LS}-A^{J(0)}_{LS}]$$

and

$$^{+}W^{J}_{LS}=2qq'\frac{J+2}{2J+3}[A^{J+2,(0)}_{LS}-A^{J(0)}_{LS}].$$

[33] H. P. Stapp, T. J. Ypsilantis, and N. Metropolis, Phys. Rev. **105**, 302 (1957).
[34] V. G. J. Stoks, R. A. M. Klomp, M. C. M. Rentmeester, and J. J. de Swart, Phys. Rev. C **48**, 792 (1993).
[35] R. A. Arndt, I. I. Strakovsky, and R. L. Workman, computer code SAID, Scattering Analysis Interactive Dial-in computer facility, Virginia Polytechnic Institute and George Washington University, solution SM99, 1999; for more information see, e.g., R. A. Arndt, I. I. Strakovsky, and R. L. Workman, Phys. Rev. C **50**, 2731 (1994).
[36] R. Machleidt, K. Holinde, and Ch. Elster, Phys. Rep. **149**, 1 (1987).
[37] Note that the Bonn model uses the πNN coupling constant $g^2_{\pi NN}/4\pi=14.4$, while for chiral pion exchanges we apply $g^2_{\pi NN}/4\pi=13.6$ (cf. footnote a of Table I). This is the main reason for the light ''discrepancies'' between N3LO and Bonn that seem to show up in some of the *H* waves (Fig. 9).
[38] In fact, preliminary calculations, which take an important class of diagrams of fifth order into account, indicate that the N^4LO contribution may prevailingly be repulsive [N. Kaiser (private communication)].
[39] G. E. Brown and A. D. Jackson, *The Nucleon-Nucleon Interaction* (North-Holland, Amsterdam, 1976).
[40] R. Vinh Mau, in *Mesons in Nuclei*, edited by M. Rho and D. H. Wilkinson (North-Holland, Amsterdam, 1979), Vol. I, p. 151; M. Lacombe, B. Loiseau, J. M. Richard, R. Vinh Mau, J. Côté, P. Pires, and R. de Tourreil, Phys. Rev. C **21**, 861 (1980).
[41] E. Epelbaum, A. Nogga, W. Glöckle, H. Kamada, U.-G. Meißner, and H. Witala, ''Few-Nucleon Systems with Two-Nucleon Forces from Chiral Effective Field Theory,'' nucl-th/0201064.
[42] M. Chemtob, J. W. Durso, and D. O. Riska, Nucl. Phys. **B38**, 141 (1972); A. D. Jackson, D. O. Riska, and B. Verwest, Nucl. Phys. **A249**, 397 (1975).
[43] R. Vinh Mau, J. M. Richard, B. Loiseau, M. Lacombe, and W. M. Cottingham, Phys. Lett. **44B**, 1 (1973); M. Lacombe, B. Loiseau, J. M. Richard, R. Vinh Mau, P. Pires, and R. de Tourreil, Phys. Rev. D **12**, 1495 (1975).
[44] We note that in the Nijmegen analysis [21] $c_4=4.7\pm0.7$ GeV^{-1} emerges which also differs from what we use and what is obtained in πN analysis (cf. Table I). However, this difference in c_4 has very little impact on *NN* peripheral partial waves and does not make possible stronger values for c_3.